Proceedings of ASME IMECE:
2002 ASME International Mechanical Engineering Congress and Exposition
November 17-22, 2002, New Orleans, LA

IMECE2002-39364

PROCESSING AND PROPERTIES OF NANOSTRUCTURED MAGNETIC MATERIALS

D. Kumar, S. Yarmolenko, and J. Sankar
Center for Advanced Materials and Smart Structures, Department of Mechanical Engineering, North Carolina A & T State University, Greensboro, NC 27411

J. Narayan, A. Tiwari, H. Zhou, C. Jin, and A.V. Kvit
Center for Advanced Materials and Smart Structures, Department of Materials Science and Engineering North Carolina State University, Raleigh, NC 27695

S.J. Pennycook and A. Lupini
Solid State Division, Oak Ridge National Laboratory, Oak Ridge, TN 37831

ABSTRACT

We report here a novel thin film processing method based upon pulsed laser deposition to process nanocrystalline materials with accurate size and interface control with improved mechanical and magnetic properties. Using this method, single domain nanocrystalline Fe and Ni particles in 5-10 nm size range embedded in amorphous alumina as well as crystalline TiN have been produced. By controlling the size distribution in confined layers, it was possible to tune the magnetic properties from superparamagnetic to ferromagnetic behavior. Magnetic hysteresis characteristics below the blocking temperature are consistent with single-domain behavior. The paper also presents our results from investigations in which scanning transmission electron microscopy with atomic number contrast (STEM-Z) and energy loss spectroscopy (EELS) were used to understand the atomic structure of Ni nanoparticles and interface between the nanoparticles and the surrounding matrices. It was interesting to learn from EELS measurements at interfaces of individual grains that Ni in alumina matrix does not from an ionic bond indicating the absence of metal-oxygen bond at the interface. The absence of metal-oxygen bond, in turn, suggests the absence of any dead layer on Ni nanoparticles even in an oxide matrix.

INTRODUCTION

Nanoscale magnetism currently provides a wealth of scientific interest and of potential applications [1-5]. When the size of magnetic particles is reduced to a few tens of nanometers, they exhibit a number of outstanding physical properties such as giant magnetoresistance, superparamagnetism, large coercivities, high Curie temperature, and low saturation magnetization as compared to the corresponding bulk values. Due to realization of these outstanding physical properties upon size reduction, magnetic nanoparticles are bringing revolutionary changes in a variety of applications. In view of the technological importance of producing magnetic nanocomposites, the synthesis of magnetic systems with characteristic nanoscale dimension has attracted a lot of research attention.

Inert gas condensation, sputtering, mechanical attrition, aerosol, ball milling, etc. are some of the common methods adopted to synthesize ultafine magnetic particles [6-9]. While most of these methods have met with considerable success, producing heterogeneous magnetic materials in a controlled compositional, structural and reproducible manner is still not satisfactory. One of the most common problems encountered in these methods is the concurrent coarsening of grains in close contact with each other during the annealing process. The annealing process is usually required to overcome the energy barrier for diffusion and superlattice ordering. The grain coarsening and interaction among the particles will have adverse effect on the performance of the recording media. It has been reported that physical gaps of 2-5 nm appear to be sufficient to decouple the magnetic grains. It is in this context that we have developed a laser assisted method to produce nanocrystalline materials, physically well separated from each other, in an amorphous matrix. It is advantageous to have magnetic nanoparticles separated by well-characterized physical gaps, which can prevent grain coarsening during mutlilayer thin film depositions and eliminate (or greatly reduce) interaction between the particles. The method is generic in nature and, can be applied to the synthesis of magnetic, optical, mechanical, and electroluminescent fine particles. In this paper, however, we will focus solely on the fabrication and properties of magnetic nanocrystalline iron particles in an

amorphous alumina matrix, and compare these results from the particles embedded in crystalline TiN matrix.

EXPERIMENTAL

Nanocrystalline iron and nickel particles were embedded in alumina matrix by laser ablation. A multitarget pulsed laser deposition system was used where iron/nickel and alumina targets are alternately ablated. The depositions were carried out on silicon substrates in a high vacuum environment (~5 X 10^{-7} Torr). The substrate temperature was approximately 500 ^{O}C. The energy density and repetition rate of the laser beam used were 2J/cm^2 and 10 Hz. The size of the Fe and Ni particles were controlled by selecting the deposition time of magnetic materials and insulating matrix and the deposition temperatures (see Table 1). The numbers of alternating layers (Fe and Ni and Al_2O_3) were 5. We have also deposited Ni nanocrystals in single-crystal films of TiN grown epitaxially on Si(100). The size distribution of Fe and Ni particles and the crystalline quality of both the matrix and magnetic particles were investigated by cross-sectional high-resolution transmission electron microscopy (HRTEM). The magnetic properties of Fe-Al_2O_3 systems were measured using superconducting quantum interference device (SQUID) magnetometer. The size of Fe/Ni nanocrystals was determined by the amount of laser deposited iron. The zero field cooled (ZFC) magnetization was achieved by applying a small field ranging from 50 to 500 Oe to the sample at 10 K and then warming the sample in the constant field with the magnetization being measured as a function of temperature. The field cooled (FC) magnetization was measured by cooling the sample to 10 K in presence of 50 Oe to 500 Oe field and taking the data while heating the samples up to 300 K. The coercivity of each sample was measured by recording magnetization versus field loops at different temperatures.

RESULTS AND DISCUSSION

Studies of Fe nanoparticles embedded in thin film Al_2O_3 matrix

Microstructural Characterization

Figure 1 shows a cross-section HRTEM micrograph for a Fe-Al_2O_3 sample where the average size of Fe nanocrystallites embedded in amorphous alumina was determined to be 9 nm. The average intralayer separation between two Fe nanocrystallites is found to be about 2.5 nm. The crystalline nature of Fe nanoparticles in amorphous alumina matrix is clearly evident. The Fe nanocrystals are randomly orientated because they nucleate in an amorphous alumina matrix.

Effect of particle size and temperature on coercivity

Shown in Fig. 2 is the M-H loops at 300 K for Fe-Al_2O_3 samples having three different Fe particles sizes. The particle size of Fe in these samples are 4.5, 7 and 9 nm, respectively from TEM studies. As seen in this figure, the coercivity decreases from 100 to 50 Oe as the particle size decreases from 9 nm to 7 nm and finally the sample turns superparamagnetic when the Fe particle size becomes ~5 nm.

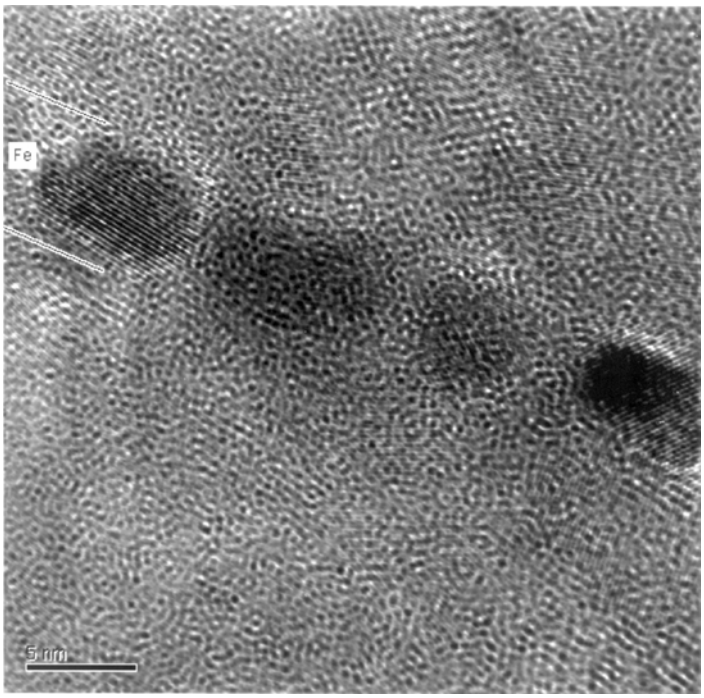

Figure 1. Cross section HRTEM recorded from a typical Fe embedded alumina thin film composite sample.

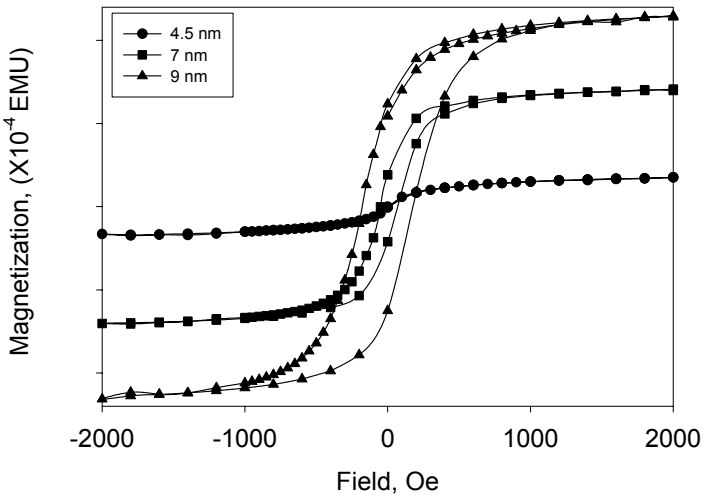

Figure 2. M-H plots for Fe-Al_2O_3 samples with three different particle sizes at 300 K.

Figure 3 shows the variation of the coercivity with temperature for Fe-Al_2O_3 samples having different Fe particle sizes. It is apparent from this figure that the coercivity is strongly dependent on temperature. This is because in order for a particle to reverse its spin, it should have enough thermal energy to surmount the energy barrier $\Delta E = KV$ for the reversal,

where K is anisotropy constant and V is the volume of a particle. The energy barrier for the reversal is the difference the maximum and minimum values of the total energy *(E)*. At higher temperature, the particles have higher thermal energy, and hence, they require smaller magnetic fields to reverse the magnetization. This field is equal to coercivity (H_c) and is given by [10]

$$\mathbf{H_c = \frac{2K}{M_S}\left[1-\left(\frac{25k_BT}{KV}\right)^{1/2}\right]} \qquad (1)$$

When *T* approaches zero, H_c approaches $2K/M_s$ *i.e.,*$H_{c,0} = 2K/M_s$, where M_s is the saturation magnetization. For particles of constant size there is a temperature, called the blocking temperature, T_B, at which the metastable hysteretic response is lost for a particular experimental time. For uniaxial particles T_B can be taken as $KV/25k_B$. Substituting the value of T_B and $H_{c,0}$ in equation (1), we get

$$\mathbf{H_c = H_{c,0}\left[1-\left(\frac{T}{T_B}\right)^{1/2}\right]} \qquad (2)$$

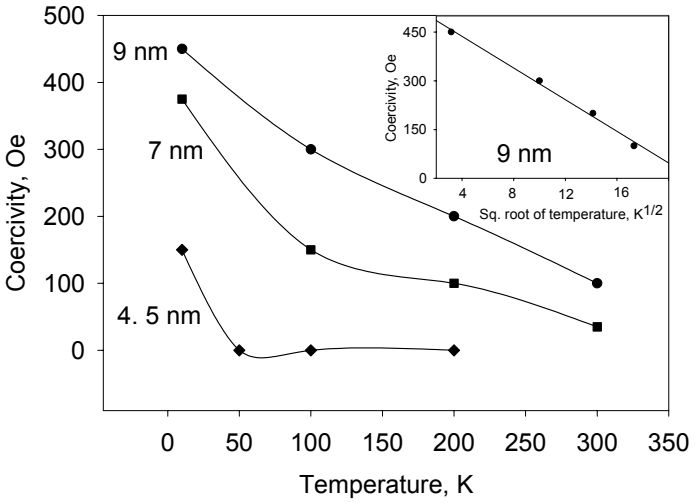

Figure 3. Variation of coercivity with temperature for Fe-Al_2O_3 samples having different Fe particle sizes. The inset shows that the iron particles follow closely $H_c = H_{c,0}\ [1-T/T_B)^{1/2}]$ relationship.

As shown in the inset of Fig. 3, the iron particles, for example, with particle size of 9 nm (sample 3) follow closely this relationship. It is clear from this figure that the fitting is pretty satisfactory and the values of parameters such as $H_{c,0}$ and T_B are very reasonable. For example, the value of T_B from this fit is found to be 481 K for this sample. Substituting the values of T_B (481 K), magnetic anisotropy K (4.8 x 10^5 erg/cm^3) for Fe, and the Boltzmann constant k_B (1.38 x 10^{-16} erg/K) in the expression for $T_B = KV/25k_B$, we find the mean radius of Fe particles to be 9.38 nm. This is in good agreement with the particle size of sample 3 measured using TEM studies (Fig. 1). These results, therefore, suggest that magnetic properties of a metal ceramic composite can be tuned in a controlled fashion by changing the particle size and temperature. The presence of single domain regions are responsible for these high values of H_c where magnetization reversal takes place only by rotation of saturation magnetization *(M_s)* vector in accordance with the Stoner and Wohlfarth model [10-13]. For spherical single-domain particles of iron with their easy axis aligned with the field, the intrinsic coercivity given by $2K/M_s$, is equal to *560 Oe*, which is closed to the experimental value we have obtained in the present study.

FC and ZFC magnetization

Shown in Fig. 4 is the FC and ZFC magnetization as a function of temperature for three Fe-Al_2O_2 samples with different Fe particles size.

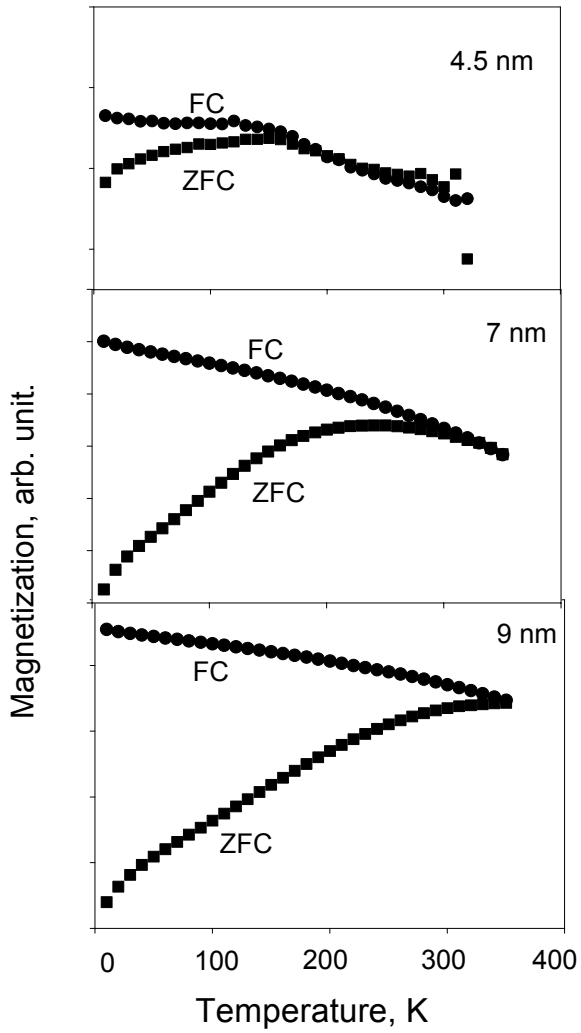

Figure 4. FC and ZFC magnetization as a function of temperature for three Fe-Al_2O_2 samples with different Fe particles size.

For the ZFC magnetization, the samples were cooled to 10 K in the absence of magnetic field. A field of 500 Oe was then

applied and the magnetization was measured as the sample was heated up to 350 K. The FC magnetization was measured by cooling the sample to 10 K in presence of 500 Oe field and taking the data while heating the samples up to 350 K. It is clear from this figure that the ZFC and FC magnetization bifurcates at different temperatures in different samples. The temperature at which this bifurcation occurs is regarded as the experimentally measured blocking temperature of each sample. The blocking temperature of sample # 3 (particle size 9 nm) is highest as the FC and ZFC magnetization curves do not overlap up to 350 K. The blocking temperatures of sample 1 (particle size 4.5 nm), and sample 2 (particle size 7 nm) are about 60 and 280 K, respectively. These values are also supported by the disappearance of magnetic hysteresis in respective sample at temperatures higher than experimentally measured T_B.

A more detailed M vs T measurement has also been carried out, as shown in Fig.5 for sample #2 (particle size 7 nm) by applying several different fields. It is clear from these plots that the temperature at which FC and ZFC bifurcation takes place is a strong function of the field in which the magnetization is measured. If the deviation in FC and ZFC curves is the blocking temperature, then T_B of this sample are approximately 190, 260, 290 and 300 K corresponding to 500, 200, 100 and 50 Oe fields, respectively. At all the fields, the FC magnetization is smaller that the ZFC magnetization. The smaller ZFC magnetization may be associated with the relaxation of magnetic moments.

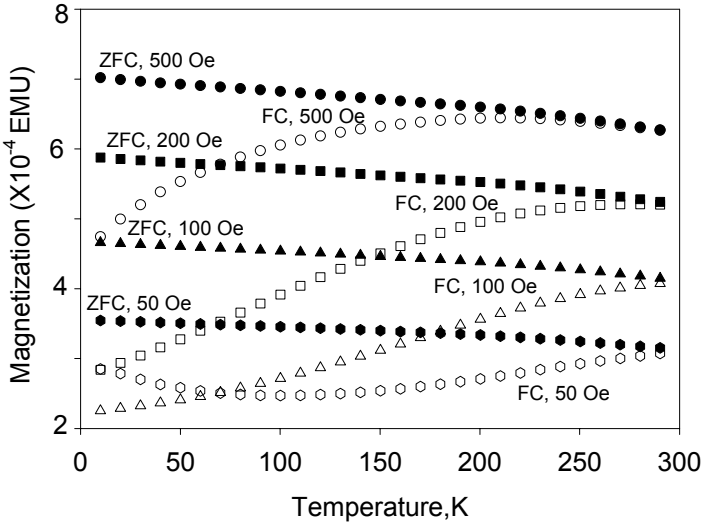

Figure 5. FC and ZFC M vs T measurements for sample #2 by applying several different fields.

Studies of Ni nanoparticles embedded in amorphous Al_2O_3 and epitaxial TiN thin film matrices

Microstructural Characterization

The cross sectional STEM-Z image of Ni particles in TiN matrix (Fig. 6a) have shown that the metallic particles are well separated (~10 nm) from each other. Shown in Fig. 6 (b) is a high-resolution STEM image of a triangular precipitate in <110> cross-section. The average size of the Ni nanodots was found to be around 17 nm base and 9nm height. As seen in Fig. 6(b), the Ni nanodots in TiN matrix have two distinct epitaxial relationships: 1) cube-on-cube <001> Ni//<001>TiN/Si with dots having a rectangular morphology; and 2) Ni dots having 90^o rotation with respect to [110] TiN with a triangular morphology.

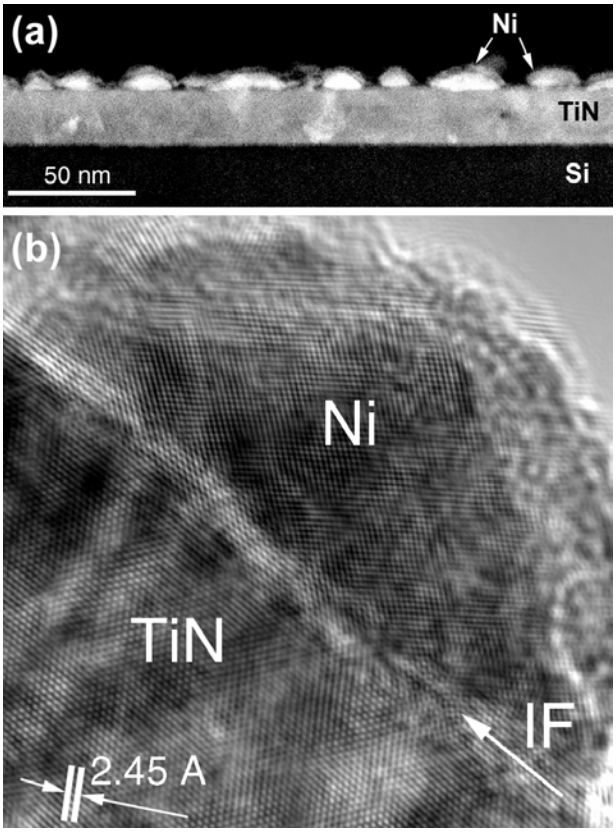

Figure 6. (a) Cross sectional STEM-Z image of Ni particle in TiN matrix and (b) High resolution TEM of one of the particles shown in (a).

Due to chemical reactivity of Ni with oxygen, one may possibly speculate an oxidation of Ni particles to some extent, especially in the oxide (Al_2O_3) matrix. Electron energy loss (EEL) spectra collected on a 100 kV HB501UX STEM confirm that no oxide shell was formed. Spectra were obtained while scanning a line across the particle and acquiring the annular dark field signal simultaneously. In this way, the position of the probe for each EEL spectrum was known to atomic precision. The energy resolution of the parallel energy loss spectrometer, as determined by the full-width half-maximum of the zero-loss peak, was 1.1 eV and the dispersion was 0.303 eV/channel over 385 channels. Each spectrum was corrected for the gain variation across the detector array and the background was fitted to a power law over a 50 eV window

preceding the edge-onset and subtracted from each spectrum. Spectra from the center and edge of a single Ni particle are displayed in Fig. 7. We used the ratio of L_2 and L_3 EELS edges as a signature of Ni since its fine structure is very sensitive to the valence state of the Ni. The L_3/L_2 ratio of Ni^{2+} is 20-30 % higher than that of metallic Ni. The L_3 peak is also much sharper and more symmetrical in NiO than Ni due to the presence of a core exciton in the oxide. We estimate less than 0.1 monolayer of oxide based on the statistics in the spectra. Shown in this figure is also the background spectrum which was subtracted from both of the center and edge spectra.

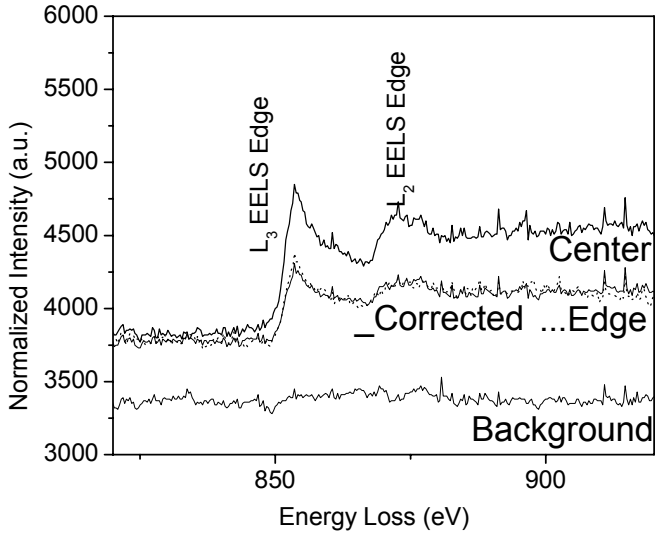

Figure 7. EEL Spectra from the center and edge of a single Ni particle. Shown also is the background spectrum.

Magnetization versus temperature measurements

Shown in Fig. 8 are the ZFC and FC magnetization data as a function of temperature for Ni- Al_2O_3 (Fig. 8 a) and Ni-TiN (Fig. 8b) samples. The average size of Ni particles were similar in both of the samples. It is clear from these figures that ZFC and FC curves are irreversible for both the samples below a certain temperature and the temperature at which the irreversibility set in are quite different from each other. The ZFC and FC curves clearly diverge from each other at 100 K for Ni-Al_2O_3 and at 275 K for Ni-TiN sample. Below these respective temperatures, the ZFC curves for both of the samples reach a maximum. According to Fig. 8, the T_B's of Ni nanocrystallites are ~30 and 190 K in Al_2O_3 and TiN matrices, respectively. Ideally the blocking temperature and the temperature at which the irreversibility sets in ZFC and FC magnetization should be the same. The difference in the two temperatures is attributed to the size distribution and relative orientation of magnetic particles having different T_B.

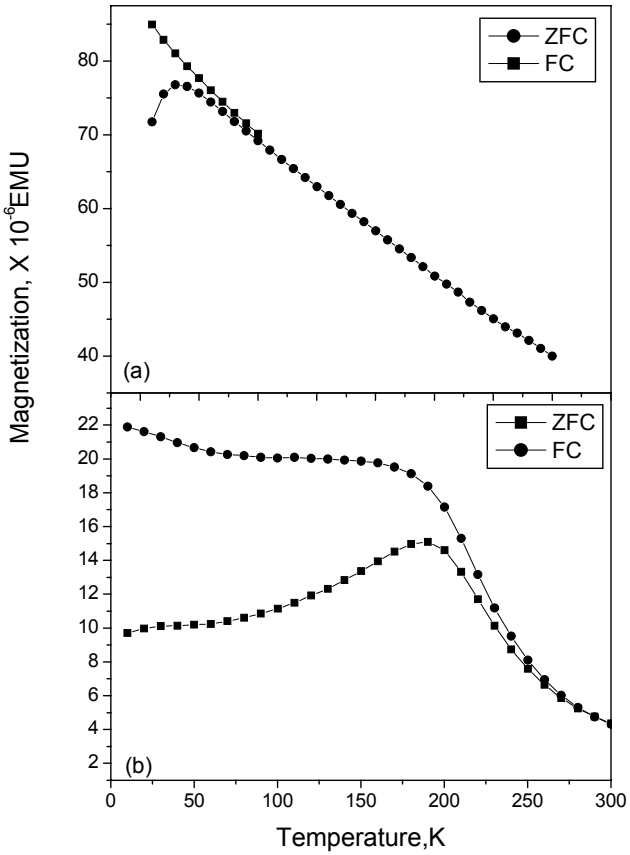

Figure 8. ZFC and FC for Ni particles in (a) alumina and (b) TiN matrices.

The high value of T_B of Ni-TiN sample with respect to T_B of Ni-Al_2O_3 sample is believed to be associated primarily with the texturing of Ni particles, which in turn influences the anisotropy energy of the system. The Ni-particles in Ni-TiN samples are epitaxial while they (Ni) are polycrystalline in Ni-Al_2O_3 sample. The Ni particles in Ni-TiN sample grow epitaxially via domain epitaxy as the TiN acting as a template also grows epitaxially on Si substrate via domain epitaxy where four lattice constants of TiN match with three of silicon. On the other hand, Ni particles in Ni-Al_2O_3 is polycrystalline due to amorphous alumina substrate. The textured nanoparticles are expected to have higher anisotropy energy. It is known that the magnetization vector in a magnetically ordered material undergoes reversals below the magnetic ordering temperature as a result of thermal excitation over the anisotropy energy. Due to this the blocking temperature, above which thermal excitation will strongly cause reversals of the magnetization vector almost instantaneously, will be higher in for textured magnetic nanocrystals.

Magnetization versus field measurements

Fig. 9 shows the magnetization versus field curves for Ni-Al_2O_3 and Ni-TiN samples. The values of H_c, noted from these

curves, are found to be 25, 45, 125, 270, and 550 Oe at 300, 200, 100, 50, and 10 K, respectively for Ni-TiN sample. The Ni-Al_2O_3 sample exhibits a coercivity of ~150 Oe at 10 K and it is almost superparamagnetic beyond 100 K which is in accordance with blocking temperature of Ni-Al_2O_3 sample measured from the M-T plot.

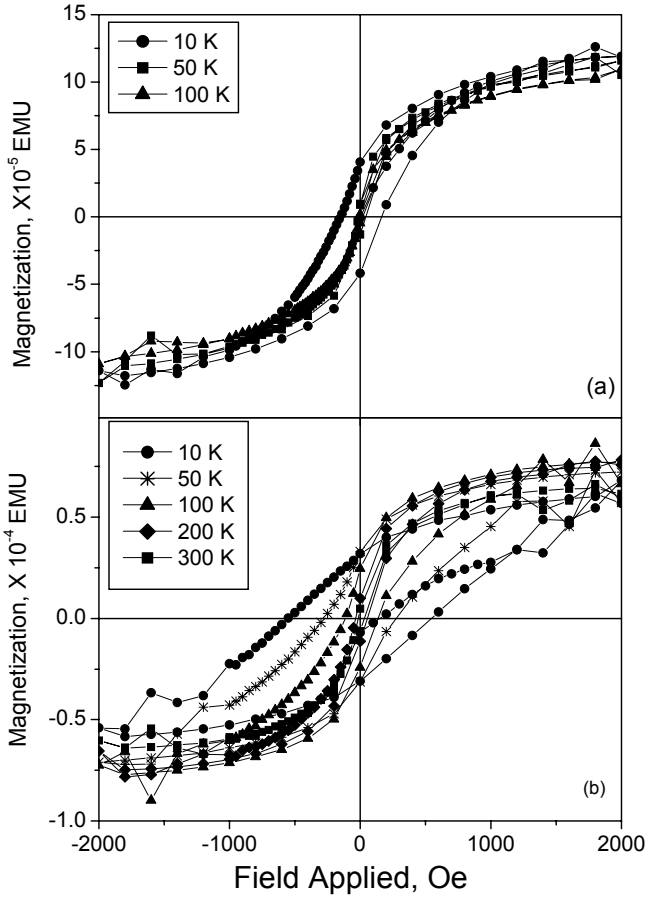

Figure 9. Magnetization versus filed curves for Ni particles in (a) alumina and (b) TiN matrices.

A simple comparison of the values of coercivity of the two samples indicates that epitaxial Ni particles exhibit significantly higher coercivity than polycrystalline Ni particles at a particular temperature. The high value of H_c of epitaxial Ni nanocrystals compared with polycrystalline Ni nanocrystals is envisaged to be associated with the stronger tendency of crystallographically oriented particles to retain their magnetic moments than that of randomly oriented particles under a reversing magnetic field. The higher values of H_c in cases of epitaxial samples (Ni-TiN) may also arise from the fact that the field applied during M-H measurements is off by 40^o from easy axis, which is <111> in case of Ni. As a result, the magnitude of real field applied along easy axis is H Cos40^o, which turns out to be 76 % of the total field applied. Since saturation magnetization is smaller along easy axis than along hard axes, the saturation magnetization of epitaxial magnetic particles is smaller than that of randomly oriented particles, and hence, epitaxial Ni nanocrystallites in TiN matrix possess high H_c values in comparison to randomly oriented Ni nanocrystallites in amorphous Al_2O_3 matrix .

An estimate of the average magnetic size is obtained from the slope of the magnetization near zero field, the major contribution to which comes from the largest particles. Therefore, an upper bound for the magnetic size may be estimated using the M-H data at 100 K (Fig. 9a) and the following equation (Cullity, 1972),

$$D_m = \left[\frac{18 k_b T}{\pi} \frac{\left(dM/dH \right)_{H=0}}{\rho M_s^2} \right]^{1/3}, \qquad (3)$$

where D_m is the maximum diameter, k_b is the Boltzmann constant, T is the temperature (100 K), dM/dH = slope near zero field (0.175 emu/g Oe), and is ρ the density of Ni (8.9 g/cm^3). The initial slope near origin was determined from the hysteresis plots by curve-fitting the linear portion of the data. Inserting the value of saturation magnetization M_s from the above curve fitting (67 emu/g), the magnetic diameter of the particle is found to be 7 nm. This is exactly the same as the diameter of the particles measured using STEM-Z images. Such an excellent correlation between the magnetic size and the physical size of the particles indicates the absence of any magnetically dead layer on the Ni particles.

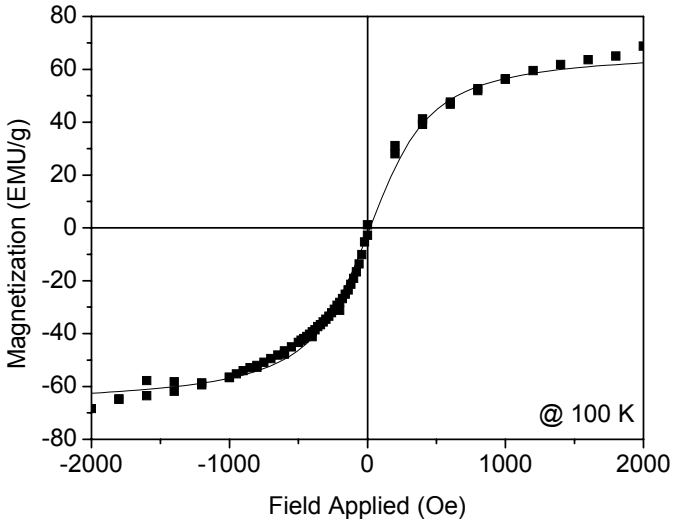

Figure 10. The best fit for the Langevin function at 100 K.

Above the blocking temperature, the typical characteristics of superparamagnetic behavior are observed showing almost immeasurable coercivity and remanence at 50 and 100 K (Fig. 9a). For superparamagnetic particles, the true magnetic moment at a particular temperature can be calculated using the Langevin function (Cullity, 1972)

$$M = M_s\left(\coth\left(\frac{\mu H}{k_b T}\right) - \frac{k_b T}{\mu H}\right), \qquad (4)$$

where μ is the true magnetic moment of each particle, k_b is the Boltzmann constant, T is the absolute temperature and M_s is the saturation magnetization. Fig. 10 shows the best fit for the Langevin function in equation at 100 K. From this data fitting, the mean-magnetic moment per Ni nanocrystal is found to be 9074 μB, which yields a magnetic moment of 0.64 μB per atom. This value of magnetic moment per atom is in excellent agreement with the theoretical value of magnetic moment of Ni atom at (0.60 μB per atom).

CONCLUSIONS

We have developed a laser assisted method to produce nanocrystalline materials, physically well separated from each other, in amorphous and crystalline matrices. It is advantageous to have magnetic nanoparticles separated by physical gaps, which prevent grain coarsening during mutlilayer thin film depositions and eliminate (or greatly reduce) interaction between the particles. In view of the technological importance of producing magnetic nanocomposites, the synthesis of magnetic systems with characteristic nanoscale dimension is very useful. The presence of single domains is believed to be responsible for high values of H_c where magnetization reversal takes place only by rotation of saturation magnetization vector. We have also shown the orientation dependence of magnetic properties of nanoparticles, which can be used to optimize the properties of nanostructured composites.

ACKNOWLEDGMENT

We are to acknowledge a partial support of the National Science Foundation, through the Center for Advanced Materials and Smart Structures.

REFERENCES

[1] Kumar, D., Narayan, J., Kvit , A.V., Sharma, A.K., and Sankar, J., J. Magnetsim and Magnetic Materials, 2001, Vol. 232 2001, pp. 161-167.

[2] Gu, E., Ahmad, E., Gray, S.J., Daboo, C., Bland, J.A.C., Brown, L.M., and Chapman, J.C., Physical Review Letters, 1997, Vol. 78 pp. 1158-1161.

[3] Fruchart, O., Nozieres, J.P., Wernsdorfer, W., Givord, D., Rousseaus,F., and Decanini, D., Physical Review Letters, 1999, Vol. 82, pp. 1305-1308.

[4] Lu, L, Sui, M.L., Science, 2000, Vol. 287, pp. 1463-1467.

[5] Prinz,G.A., Science, 1998, Vol. 282, pp. 1660-1662.

[6] Kumar, D., Zhou, H, Nath, T.K., Kvit, A.V., and Narayan, J., Applied Physics Letters, 2001, Vol. 79, pp. 2817-2819.

[7] Mehn, Punadjela, K., Bucher, J., Roussseausx, F., Decanini, D., Bartenlian, B., and Chappert, C., Science, 1996, Vol. 272, pp. 1782.

[8] Yu, J., Rudiger, U., Thomas, L., Parkin, S.S.P., and Kent, A.D., Journal of Applied Physics, 1999, Vol. 85, pp. 5501-5507.

[9] Xu, Y.B., Hirohata, A., Diaz, L.L., Leung, H.T., Tselpi, M., Gardiner, S.M, Lee, W.Y., Bland, J.A.C., Rousseaux, F., Cambril, E., and Launois, H., Journal of Applied Physics, 2000, Vol. 87, pp. 7019-7023.

[10] Cullity, B.D., in "Introduction to Magnetic materials", Addison Wesley Publishing Company, Massachusetts, 1972.

[11] Schultz, L., Schnitzke, K., and Wecker, J., Applied Physics Letters, 1990, Vol. 56, pp. 868-870.

[12] Kumar, D., Narayan, J., Nath, T.K., Sharma, A.K., Kvit, A., Jin, C., Solid State Communications, 2001, Vol. 119, pp. 63-64.

[13] Akinaga, H., Miyanishi, S., Tanaka, K., Van Roy W., and Onodera, K., Applied Physics Letters, 2000, Vol. 76, pp. 97-99.